NeuroImage: Clinical 21 (2019) 101596

Contents lists available at ScienceDirect

NeuroImage: Clinical

journal homepage: www.elsevier.com/locate/ynicl

White matter injury predicts disrupted functional connectivity and microstructure in very preterm born neonates

Emma G. Duerden[a,e], Sheliza Halani[a], Karin Ng[a], Ting Guo[a], Justin Foong[a], Torin J.A. Glass[a], Vann Chau[a,c], Helen M. Branson[a], John G. Sled[b,c], Hilary E. Whyte[a], Edmond N. Kelly[c,d], Steven P. Miller[a,b,c,*]

[a] Department of Paediatrics, The Hospital for Sick Children, 555 University Avenue, Toronto, ON M5G 1X8, Canada
[b] Research Institute, Hospital for Sick Children, 686 Bay St, Toronto, ON M5G 0A4, Canada
[c] The University of Toronto, 27 King's College Circle, Toronto, ON M5S 1A1
[d] Department of Paediatrics, Mount Sinai Hospital, 600 University Ave, Toronto, ON M5G 1X5, Canada
[e] Faculty of Education, The University of Western Ontario, 1137 Western Rd, London, ON, N6G 1G7, Canada

ARTICLE INFO

Keywords:
Preterm birth
Resting-state networks
Diffusion tensor imaging
Connectivity
Human

ABSTRACT

Objective: To determine whether the spatial extent and location of early-identified punctate white matter injury (WMI) is associated with regionally-specific disruptions in thalamocortical-connectivity in very-preterm born neonates.

Methods: 37 very-preterm born neonates (median gestational age: 28.1 weeks; interquartile range [IQR]: 27–30) underwent early MRI (median age 32.9 weeks; IQR: 32–35), and WMI was identified in 13 (35%) neonates. Structural T1-weighted, resting-state functional Magnetic Resonance Imaging (rs-fMRI, $n = 34$) and Diffusion Tensor Imaging (DTI, $n = 31$) sequences were acquired using 3 T-MRI. A probabilistic map of WMI was developed for the 13 neonates demonstrating brain injury. A neonatal atlas was applied to the WMI maps, rs-fMRI and DTI analyses to extract volumetric, functional and microstructural data from regionally-specific brain areas. Associations of thalamocortical-network strength and alterations in fractional anisotropy (FA, a measure of white-matter microstructure) with WMI volume were assessed in general linear models, adjusting for age at scan and cerebral volumes.

Results: WMI volume in the superior ($\beta = -0.007$; $p = .02$) and posterior corona radiata ($\beta = -0.01$; $p = .01$), posterior thalamic radiations ($\beta = -0.01$; $p = .005$) and superior longitudinal fasciculus ($\beta = -0.02$; $p = .001$) was associated with reduced connectivity strength between thalamus and parietal resting-state networks. WMI volume in the left ($\beta = -0.02$; $p = .02$) and right superior corona radiata ($\beta = -0.03$; $p = .008$), left posterior corona radiata ($\beta = -0.03$; $p = .01$), corpus callosum ($\beta = -0.11$; $p < .0001$) and right superior longitudinal fasciculus ($\beta = -0.02$; $p = .02$) was associated with functional connectivity strength between thalamic and sensorimotor networks. Increased WMI volume was also associated with decreased FA values in the corpus callosum ($\beta = -0.004$, $p = .015$).

Conclusions: Regionally-specific alterations in early functional and structural network complexity resulting from WMI may underlie impaired outcomes.

1. Introduction

Very-preterm neonates (< 32 weeks' gestation) are at high-risk for white matter injury (WMI) early in life (Iwata et al., 2012; Miller et al., 2005; Woodward et al., 2006). Quantitative mapping of early identified WMI indicates that injury location rather than total volume is associated with adverse outcomes (Guo et al., 2017) and may underlie disruptions in functional- and structural-brain connectivity. In contrast, evidence from resting-state functional magnetic resonance imaging (rs-fMRI) indicates that total WMI volume and severity can selectively impact intra-cortical and subcortical functional connectivity, assessed at term in preterm neonates with severe WMI (He and Parikh 2015;

Abbreviations: fMRI, functional magnetic resonance imaging; GA, gestational age; PMA, postmenstrual age; FA, fractional anisotropy; WMI, white matter injury; DTI, Diffusion tensor imaging; MRI, magnetic resonance imaging; rs, resting state

* Corresponding author at: Hospital for Sick Children, 555 University Avenue, Toronto, ON M5G 1X8, Canada.
E-mail address: steven.miller@sickkids.ca (S.P. Miller).

https://doi.org/10.1016/j.nicl.2018.11.006
Received 31 January 2018; Received in revised form 26 October 2018; Accepted 12 November 2018
Available online 13 November 2018

Smyser et al., 2013). Thalamocortical functional connectivity may be disrupted in neonates born preterm and may be a key predictor of neurodevelopmental outcome (Smyser et al., 2010).

Additionally, clinical scores of WMI predict regionally-specific alterations in WM microstructure measured during the postnatal period and term-equivalent age in preterms (Miller et al., 2002; van Pul et al., 2012); however, the association with the spatial extent of WMI volume with microstructure and functional connectivity has not been assessed.

Given the importance of WMI in the very preterm neonate, we assessed the hypothesis that the spatial extent and location of WMI identified on early MRI was associated with regionally-specific alterations in thalamocortical-network strength and white-matter (WM) microstructure. Postnatal infection is associated with WMI in very preterm born neonates (Chau et al., 2009). In the current study, a prospective cohort of very preterm born neonates at very high risk for the exposure to infection was recruited and the association of WMI with brain structural and functional connectivity seen on MRI acquired early-in-life, at a time when injury is most readily identified, was examined. WMI was manually segmented in neonates' anatomical MRIs and transformed to create a probabilistic map in a standardized neonatal MR template, according to methods applied to MRI data acquired in a previous cohort of very preterm-born neonates (Guo et al., 2015, 2017). Resting-state fMRI data were acquired and networks were identified in neonates with and without WMI using independent components analysis. Functional-connectivity strength between thalamic and cortical resting-state networks was assessed between the groups (He and Parikh, 2015; Smyser et al., 2013). Lastly, in a complementary analysis, diffusion tensor imaging (DTI) was acquired to determine the association among DTI-metrics of white-matter microstructure in neonates with and without WMI and also with the size and location of WMI.

2. Methods

2.1. Participants

Very preterm neonates (< 32 weeks' gestational age) admitted to the neonatal intensive care units at the Hospital for Sick Children and Mount Sinai Hospital, Canada were enrolled. Research Ethics Boards at both hospitals approved the study. Neonates were included if they were born at a gestational age of 24–32 weeks, had evidence of infection (clinical or culture-positive) or were at high-risk for an infection (Stoll et al., 2004). Written informed consent was obtained from parents/legal caregivers.

Neonatal research nurses collected demographic data and clinical variables systematically.

2.2. Magnetic resonance imaging

Neonates were scanned without sedation in an incubator (Lammers Medical Technology, Luebeck, Germany) on the same Siemens (Erlangen, Germany) 3 T Tim Trio MRI scanner at the Hospital for Sick Children, Toronto using a single-channel neonatal head coil (Advanced Imaging Research, Cleveland, OH).

MRI scans were acquired early in life at a median postmenstrual (PMA) age of 32.9 weeks (IQR: 31.9–34.7). Anatomical images were acquired using a T1-weighted FLASH sequence (repetition time [TR], 36msecs; echo time [TE], 9.2 msec; field of view [FOV], 192 × 88 mm; voxel size: 1 mm isotropic). Resting-state fMRI was acquired using an echo-planar imaging sequence (TE, 50 msec, TR, 3 s, FOV, 192 mm, matrix, 64 × 64, slice thickness, 3 mm, 32 slices, 100 volumes). DTI were obtained with a single-shot echo-planar imaging sequence (TE, 86 ms, TR, 8100 ms, FOV, 160 mm, slice thickness, 2 mm, motion-probing gradient in 30 diffusion-encoding directions with a diffusion weighting of 700 s/mm^2 [*b* value] and a non-diffusion weighted image). An additional diffusion weighted image was acquired for diagnostic purposes (TE, 105msecs, TR, 5.8 s, FOV, 144 mm, slice thickness, 4 mm, 30 slices).

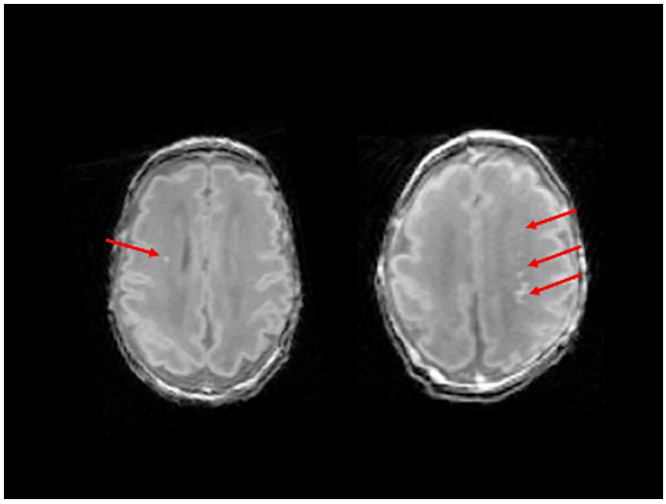

Fig. 1. Examples of punctate white mater injury (red arrows) identified in two neonates on T1-weighted images.

Anatomical images were reviewed by an experienced paediatric neuroradiologist (HMB) and a paediatric neurologist (TJAG) for the severity of intraventricular haemorrhage (IVH), periventricular leukomalacia, cerebellar haemmorhage, ventriculomegaly and for quantifying WMI volumes. WMI was seen as hyper-signal on T1-weighted MRIs. Examples are shown in Fig. 1. WMI and total cerebral volumes (TCV) were manually segmented by two of the authors (EGD, SH) using the 3D visualization software Display (http://www.bic.mni.mcgill.ca/software/Display/Display.html) in each participant's T1-weighted MRI previously described in (Guo et al., 2017). A WMI map was created from each participant's T1-weighted image in native MR space. WMI and TCV volumes were extracted.

A study-specific neonatal MRI template was created from the T1-weighted MRIs of neonates with and without WMI who participated in the study using MICe build model (https://wiki.mouseimaging.ca/display/MICePub/MICe-build-model). A probabilistic map of WMI was developed from the individual maps to examine patterns of injury, overlaid on homologous brain regions in the neonatal template (Guo et al., 2017). In brief, the individual manually-labelled WMI maps were nonlinearly registered to the common MR image space of the neonatal template to account for individual anatomical variability. The individual maps were combined to produce a probabilistic WMI map that describes the pooled incidence of WMI at each voxel in the neonatal template.

2.3. Rs-fMRI analysis

Rs-fMRI data were preprocessed using the FMRIB Software Library (FSL; version 5.0.6). Preprocessing included: slice timing and motion correction, spatial smoothing, band-pass filtering (suppressing physiological noise) and whole-brain tissue extraction. The head motion parameters for each neonate were reviewed. Datasets containing movement (> 2 mm in > 33% of volumes from the mean head position) were removed according to previously published methods employed using data obtained from very preterm born neonates (Schneider et al., 2018). As the full MRI protocol including intra- and inter-hospital transport to the scanner was 1.5–2 h, we tailored the scanning sequences to be acquired as efficiently and rapidly as possible to return the neonate to the NICU for feeding. In turn, only 5 min of resting-state data or 100 volumes (frames) were acquired in the neonates, which has been noted as the minimum amount of data to be included in a group analysis (Smyser et al., 2013). We therefore excluded entire motion-corrupted datasets rather than frames to ensure a

minimum amount of 100 scanning frames was included in the final analyses. Data were nonlinearly registered to the template.

Whole-brain resting-state connectivity was examined in neonates with and without WMI using a group temporal-concatenation independent-components-analysis (ICA), available in FSL using MELODIC (Multivariate Exploratory Linear Decomposition into Independent Components, version 4.0) (Beckmann & Smith, 2004). The number of components was determined automatically for each group. For the WMI group a total of 54 components were produced and for the no WMI group 65 components resulted from the analysis. The components were visually inspected and were discarded based on the spatial pattern and/or the frequency of the power spectrum. Visual inspection of the components involved detection of noise outside the brain or inside the ventricular spaces. Based on our a priori hypotheses regarding the association with WMI and thalamocortical connectivity, we based our selection of components on previously published literature in neonates demonstrating resting-state networks in the thalamus as well as sensorimotor, parietal and visual areas (Doria et al., 2010; Fransson et al., 2007; He and Parikh, 2016; Smyser et al., 2013). Resulting IC maps were thresholded using randomize, controlling for multiple comparisons using the false-discovery rate (Beckmann & Smith, 2004). The IC maps were visualized thresholding the z score maps at ≥ 4 in FSL.

2.4. Diffusion tensor imaging and atlas-based localization

DTI analyses were carried out using FSL library (FSL, http://www.fmrib.ox.ac.uk/fsl/) (Jenkinson et al., 2012) using previously described methods (Duerden et al., 2015). In brief, data were preprocessed, including correction for eddy-current effects, the diffusion-weighted volumes were linearly registered to one non-diffusion weighted volume (Jenkinson et al., 2002; Jenkinson and Smith, 2001) and data were masked to include only brain tissue (Smith, 2002). A diffusion tensor model was fit to the data at each voxel and to calculate voxel-wise fractional anisotropy (FA). To determine the spatial location of alterations in FA values, volumes were processed using the TBSS pipeline (Smith et al., 2006). FA images were nonlinearly aligned to a study-specific average template to calculate voxelwise statistics. Cluster-size thresholding at a level of $p < .05$ was employed, corrected for multiple comparisons.

The Johns Hopkins University (JHU) neonatal-atlas (Oishi et al., 2011) was nonlinearly registered to the WMI probabilistic map, ICA maps and the TBSS-based age-specific templates in neonatal-template space. By registering the neonatal atlas to the three main statistical images (1. WMI probability map; 2. ICA maps; 3. TBSS maps) this permitted regionally-specific statistical comparisons of the volume of WMI in specific white matter tracts in relation to functional and microstructural connectivity in the neonatal brain. The WMI volumes were extracted in cubic millimeters from the individual WMI probability maps using the neonatal atlas. Similarly, the fractional anisotropy (FA) values were extracted from the WM fibre pathways in the JHU-atlas (40 bilateral regions) for each participant's TBSS map.

2.5. Statistical analysis

Statistical analysis was performed using the Statistical Package for the Social Sciences (SPSS, v24, IBM). Our first aim was to assess whether neonatal WMI would be associated with variations in resting-state network strength and DTI-metrics of white matter microstructure by performing between-group (WMI vs. no WMI) analyses on the resting-state networks and the FA values obtained from the TBSS analyses. Neonates without WMI are an important comparison group to determine whether variations in resting-state connectivity and alterations in white-matter microstructure are associated with injury or reflect exposure to the extrauterine environment. Our second aim was to assess whether WMI volume would show an association with thalamocortical-network strength and white-matter microstructure so within-group analyses on the resting-state networks and FA values examining the association with WMI volume were performed. As we had two *a priori* hypotheses concerning the between- and within-group associations of WMI on brain function and structure, the alpha level for the statistical models addressing these hypotheses was set to 0.03, using the Bonferroni method to correct for multiple comparisons ($p = .05/2$).

To assess our first aim, using a general linear model (GLM) the WMI-group (i.e. WMI vs. no WMI) and hemispheric differences in network strength were assessed. The JHU-atlas was applied to the significant clusters, corresponding to a z score of ≥ 4 (sensorimotor, parietal, thalamic, visual networks) identified through ICA and the voxels from 62 regions of cortical and subcortical grey matter regions were compared between groups in separate GLMs for each network, which included an interaction term for hemisphere to assess laterality effects.

In neonates with WMI, to assess thalamocortical rs-connectivity strength in relation to WMI volume, correlation coefficients were calculated between BOLD time-series obtained from subcortical (thalamus) and cortical components (sensorimotor, parietal, visual networks) extracted using the JHU-neonatal-atlas for each individual participant. Subcortical-cortical correlations coefficients were then entered into a GLM with WMI volume extracted from WM tracts, adjusting for PMA at scan and TCV.

DTI measures of WM microstructure were assessed between groups (WMI versus no WMI) using generalized estimating equations (GEE) that accounted for repeated measures. The FA values, corrected for multiple comparisons, were extracted from 40 bilateral regions of interest (ROI) of cortical white matter in the JHU-neonatal atlas and were entered into the model. ROI and hemisphere (right/left) were entered into the model as within subject variables, adjusting for PMA at scan. Within the WMI group only, we assessed the relation between DTI measures of WM microstructure in relation to WMI volume. The atlas-based FA values were entered into separate GLMs and the association with the WMI volume from the corresponding WM regions was assessed, adjusting for PMA at scan.

3. Results

3.1. Clinical and demographic characteristics

A total of 37 very preterm born neonates participated (Table 1) and 13 (35%) had WMI. Neonates were assigned to WMI and no-WMI

Table 1
Characteristics for the full cohort ($N = 37$) for neonates with and without white matter injury (WMI).

Characteristic	WMI	No WMI	p value
	$n = 13$	$n = 24$	
Birth GA Median Weeks (IQR)	28.1 (27–30.6)	28 (26.4–28.9)	0.2
Male, No. [%]	10 [77]	16 [67]	0.7
PMA at MRI (IQR)	32.3 (31.9–32.6)	33.3 (32.4–35)	0.2
PMA at MRI range	30.9–38.9	30.4–38.6	
WMI mm^3† (SD)	4.5(8.03)	–	
PVL [%]	2 [15]	–	
IVH†† [%]	7 [54]	8 [33]	0.5
Cerebellar haemorrhage [%]	0	4 [17]	0.3
Ventriculomegaly [%]	1 [8]	1 [4]	0.4
Infection			
Clinical sepsis	3 [23]	12 [50]	0.4
Culture positive infection	6 [46]	9 [38]	
Histological chorioamnionitis	2[a] [15]	2[b] [8]	0.6

Probability values provide results using *t*-test for continuous measures and Chi-square tests for categorical measures comparing the data from neonates with and without WMI. GA, gestational age; PMA, postmenstrual age; IQR, interquartile range; SD, standard deviation; IVH, intraventricular haemorrhage; PVL, Periventricular leukomalacia; mm, millimeters; †mean WMI volume; †† grade 2–4 IVH; a, one infant also had a culture positive infection; b, one infant also had a clinical infection.

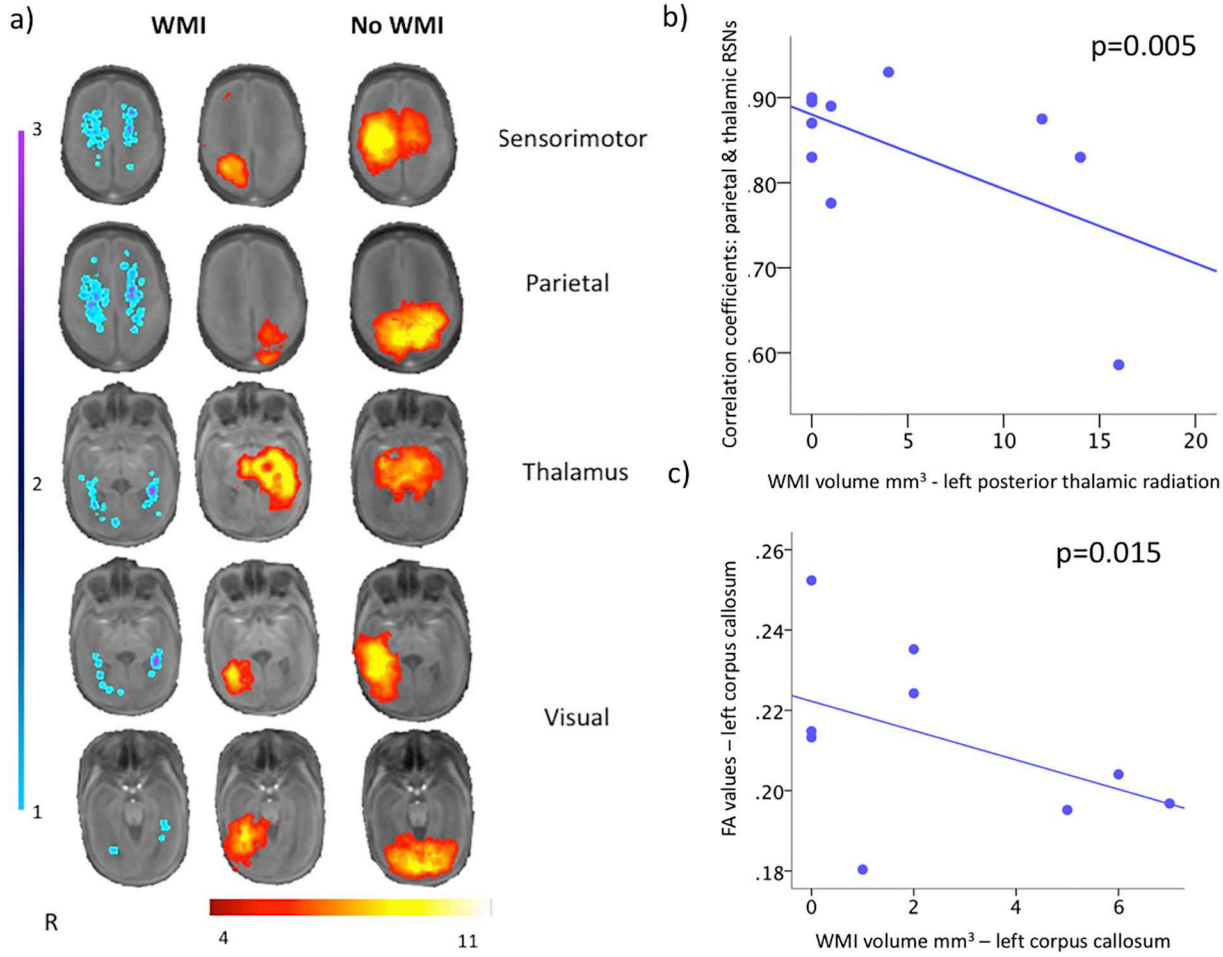

Fig. 2. a) White matter injury probabilistic map (left), and resting-state networks, group analysis for neonates with (middle) and without (right) white-matter injury (WMI) displayed on the study-specific template MRI in identical locations on axial slices. For the neonates with WMI (left) the probabilistic map describing the spatial extent and location of injury in 13 neonates is overlaid on the template MRI with the resting-state networks acquired within the first weeks of life. Warmer colours (purple) represent a higher overlap of WMI pooled across participants occurring in the same voxels in the template MRI. For display purposes, WMI volume data were smoothed using a blurring kernel of 2 mm full width half maximum.

Probabilistic independent components analysis detected sensorimotor, parietal and visual networks in the neonates with and without WMI. Similarly, a resting-state network was identified in the thalamus in both groups. However, neonates without WMI injury displayed reduced complexity in the resting-state networks compared to the no WMI group.

b) Neonates with greater volume of WMI show decreased thalamocortical connectivity strength. Correlation coefficients representing the strength of the connectivity between parietal and thalamic resting-state networks (RSNs) regressed against WMI volume extracted from the left posterior thalamic radiations using a general linear model ($\beta = -0.01$; $p = .005$), adjusting for PMA at scan and TCV.

c) Greater WMI volume in the corpus callosum was associated with decreased fractional anisotropy (FA) values extracted from the same region using the JHU-neonatal atlas ($\beta = -0.004$; $p = .015$).

groups based on the presence of punctate white matter lesions identified on MRI. The majority of neonates ($n = 32$ [86%]) had a clinical infection, a culture positive infection or were exposed antenatally to chorioamnionitis.

3.2. Spatial extent and location of WMI

Probabilistic mapping of WMI confirmed the pattern of injury occurred in the periventricular region (Fig. 2a). WMI volumes were extracted using the JHU-atlas. The incidence of WMI was localized to the left and right superior corona radiata, corpus callosum and thalamic radiations as well as the left posterior corona radiata and the right superior longitudinal fasciculus. While injury volume was largest in the right posterior thalamic radiation, GLMs applied to the data revealed that neither the average WMI volume ($\chi^2 = 3.6$, df = 3, p = .3, Table 2) nor its lateralization ($\beta = 0.3$, df = 1, p = .9) differed significantly among the measured WM fibre pathways, controlling for TCV.

3.3. Resting-state networks in neonates with and without WMI

Data from a total of 10 neonates with WMI and 24 neonates without WMI having reliable rs-fMRI data were analyzed. Resting-state data from three neonates were removed as the majority of the data were motion corrupted. The motion parameters based on the relative mean displacement were 0.0136 mm (range = 0.002–0.07 mm) for the 10 neonates with WMI and 0.0155 mm (range = 0.001–0.08 mm) for the 24 neonates without WMI. No significant differences in the mean displacement values between groups were evident (p = .9).

Sensorimotor, parietal, visual, thalamic resting-state networks were detected in both groups and were qualitatively similar (Fig. 2a). We assessed the spatial extent of the resting-state networks and their hemispheric symmetry between WMI groups. In the sensorimotor network, no between group difference in the spatial extent of networks was evident ($\beta = 90.1$ [no WMI], df = 1, p = .6); however a significant interaction (WMI × hemisphere) for WMI group and hemisphere (determined by the atlas) analysis revealed that neonates with WMI had a

Table 2
WMI volumes extracted from white-matter fibre pathways.

	Superior corona radiata		Posterior corona radiata		Corpus callosum		Posterior thalamic radiations		p value
Mean volume mm^3	5.2		4.7		2.7		6.96	0.3	
Range	2–43		1–22		1–14		1–34		
SD	10.4		7.1		4.2		10.1		
	Right	*Left*	*Right*	*Left*	*Right*	*Left*	*Right*	*Left*	
Mean volume mm^3	4.31	6.00	4.46	5.00	3.31	2.15	9.31	4.62	0.9
Range	2–19	5–43	6–22	1–16	2–14	1–7	3–34	1–16	
SD	7.84	12.68	7.74	6.71	5.50	2.51	12.81	6.06	

Average WMI volumes in white-matter fibre pathways assessed in a neonatal template MRI. Probability values provide results using general linear models comparing WMI injury volumes extracted from the white matter fibre pathways in the JHU-neonatal atlas in neonates with WMI, adjusting for total cerebral volumes. mm, millimeters; SD, standard deviation.

greater spatial extent of activation in the right hemisphere ($\beta = 397.5$ [right], $df = 1$, $p = .01$) in comparison to the left. Similarly, for the parietal networks while no difference the spatial extent of the networks was evident between groups ($\beta = -130.7$, $df = 1$, $p = .5$) the interaction with hemisphere revealed that neonates with WMI had a greater spatial extent of the parietal network in the left hemisphere ($\beta = -463.6$, $df = 1$, $p = .01$). The thalamic networks demonstrated a between group difference with neonates with WMI having a greater spatial extent of voxels ($\beta = -319.5$, $df = 1$, $p = .003$) in comparison to neonates without WMI. However, neonates with WMI demonstrated hemispheric asymmetry in the distribution of the networks as indicated by the interaction analysis ($\beta = -402.5$, $df = 1$, $p < .001$). The visual network in neonates without WMI showed a greater spatial extent in comparison to neonates with WMI ($\beta = 364.2$, $df = 1$, $p = .02$); however no within-group hemispheric differences were evident in the visual networks (both, $p > .08$).

In none of the resting-state networks for neonates without WMI were significant hemispheric differences evident (all $p > .03$). A comparable spatial extent of resting-state activity in the left and right hemispheres was found for all four resting-state networks. Neonates without WMI demonstrated bilateral resting-state sensorimotor, parietal, thalamic and visual networks.

3.4. Spatial extent and location of WMI and thalamocortical connectivity

WMI volume in the right superior ($\beta = -0.007$; $p = .02$) and left posterior corona radiata ($\beta = -0.01$; $df = 1$, $p = .01$), right superior longitudinal fasciculus ($\beta = -0.02$; $df = 1$, $p = .001$) and left posterior thalamic radiations ($\beta = -0.01$; $df = 1$, $p = .005$ Fig. 2b), adjusting for PMA at scan and TCV, was associated with the connectivity strength between parietal and thalamic networks. Additionally, WMI volume in the left ($\beta = -0.02$; $df = 1$, $p = .02$) and right superior corona radiata ($\beta = -0.03$; $df = 1$, $p = .008$), left posterior corona radiata ($\beta = -0.03$; $df = 1$, $p = .01$), corpus callosum ($\beta = -0.11$; $df = 1$, $p < .0001$) and right superior longitudinal fasciculus ($\beta = -0.02$; $df = 1$, $p = .02$) was associated with functional connectivity strength between thalamic and sensorimotor networks, adjusting for PMA at scan and TCV.

3.5. Spatial extent and location of WMI and WM microstructure

DTI data from 6 participants (4 with WMI) were excluded due to excessive motion artifacts, leaving a total of 22 datasets from neonates without WMI and 9 with WMI. Results from the GEE indicated that no significant differences in atlas-based FA values were evident between neonates with and without WMI ($\beta = -0.005$, $df = 1$, $p = .4$), adjusting for PMA at scan. However, among the neonates with WMI, increased WMI volume in the corpus callosum was associated with decreased FA values obtained from the same region ($\beta = -0.004$, $df = 1$, $p = .015$, Fig. 2c), adjusting for PMA at scan and TCV. The FA values extracted from the other white matter tracts (superior corona radiata, posterior corona radiata, superior longitudinal fasciculus and posterior thalamic radiations) showed no significant associations with the WMI in the corresponding tracts (all $p > .054$).

4. Discussion

Using multimodal neuroimaging and quantitative mapping of early WMI in very preterm neonates, we demonstrate that WMI in parieto-temporo-occipital brain regions is associated with alterations in thalamocortical connectivity and WM microstructure, particularly in pathways subserving the parietal lobes. The spatial distribution of WMI was consistent with that described in an independent cohort using the same WMI mapping methods (Guo et al., 2017). Consistent with WMI localization in this cohort, rs-fMRI revealed that neonates with WMI had reduced intra- and interhemispheric functional connectivity strength in sensorimotor, parietal, visual and thalamic networks relative to neonates without WMI even at an early post-menstrual age. Increased injury volume in posterior WM was associated with alterations in thalamic-parietal network strength. Furthermore, WMI was associated with microstructural alterations in the corpus callosum, which may partially underlie parietal lobe connectivity (Conti et al., 1986; Iwamura, 2000).

Resting-state networks have been detected in very preterm born neonates scanned at 29 weeks PMA (Doria et al., 2010) indicating that neural activity at these young gestational ages can be imaged through neurovascular responses. Our findings were obtained in neonates scanned 30–38 weeks PMA. The majority of the neonates were critically ill at the time of scan. The brain undergoes a period of exponential development during 30 to 38 weeks PMA. In our analyses, we adjusted for the effects of age; however, it is possible that resting-state networks may have been more influenced by the data included from infants scanned at older ages. Future studies with larger cohorts may answer questions related to age at scan in relation to resting-state networks in the neonate.

During this stage of development (30–38 weeks PMA) thalamocortical networks mature (Colonnese et al., 2010). Adult networks including visual, auditory, somatosensory, motor, cerebellum, brainstem, thalamic and default mode were evident in the early preterm brain becoming more complex at later postnatal ages. Our results demonstrating visual, sensorimotor, parietal and thalamic networks at relatively comparable postmenstrual ages are largely consistent with these previous rs-fMRI findings. However, a previous report noted stronger bilateral sensorimotor, parietal and visual networks in comparison to the current study (Doria et al., 2010), although in the current study no statistical differences in bilateral network strength were noted in neonates without WMI. The differences in network strength seen between the two studies may reflect differences in illness severity of the groups of neonates being assessed. For example, variations in thalamocortical network strength have been reported in very preterm born neonates based on gestational age (Toulmin et al., 2015). Exploration of spontaneous neural activity and hemodynamics in the neonatal rodent brain

at rest confirm sporadic unilateral cortical responses that are minimally coupled to blood flow changes that later develop bilaterally in the fetal-postnatal period (Kozberg et al., 2016). The absence of auditory and default mode networks in the current cohort may be related to methodological differences, the fewer numbers of participants, or differences in the maturation of the neurophysiology of these pathways.

Our findings of *early* disrupted functional connectivity strength in neonates with WMI are in agreement with previous rs-fMRI studies of very preterm born neonates scanned at term-equivalent age (He and Parikh 2015; Smyser et al., 2013). He and colleagues reported reduced within-network functional connectivity strength in executive-control and frontoparietal networks in neonates with WMI. Additionally, total WMI volume was negatively correlated with executive-control network strength. In the current work, we did not detect executive-control resting-state networks, which may be only be functional at later post-menstrual ages. An additional consideration is that our findings of posterior WMI affecting parietal lobe function may be specific to the injury pattern seen in the current cohort, as only some neonates had very large lesions that may have had a stronger association with thalamocortical network strength.

DTI studies of very preterm born neonates with WMI have reported lower FA values in major white matter fibre pathways including the corticospinal tract (Bassi et al., 2011) and cingulum bundle (Cui et al., 2017) assessed at term-equivalent age. Serial imaging of neonates during the postnatal period to term-equivalent age indicated that WMI was associated with a less robust increase in anisotropy, consistent with dysmaturation of the white matter in regions that appear normal on conventional MRI (Miller et al., 2002). Our results expand upon previous findings through quantitative mapping of WMI based on early MRI. Our method permitted the atlas-based localization and quantification of WMI volume for purposes of direct comparison with alterations in WM microstructural alterations assessed in the early neonatal period. Reduced FA in the corpus callosum in neonates with punctate WMI may reflect brain dysmaturation (Back & Miller, 2014). Studies with neonates and neonatal animal models indicate that diffuse WMI selectively targets pre-myelinating oligodendrocytes, the precursor cells to the myelin-forming oligodendrocytes, resulting in the disruption of myelination (Haynes et al., 2008; Riddle et al., 2012). The results of this study are in agreement with previous findings in indicating that focal WMI lesions are accompanied by abnormalities along WM microstructure pathways.

The adverse consequence of WMI is not restricted to the white matter; evidence from MRI suggests that reduced myelination and cortical folding was present in preterm born neonates with WMI evident on MRI at term-equivalent age (Ramenghi et al., 2007). In an experimental model with detailed MRI and histopathology, diffuse WMI is associated with disruptions in dendritic arborization and neuronal spine formation, which may itself underlie abnormalities in cortical growth (Dean et al., 2013). Our findings of reduced intra- and interhemispheric connectivity and lack of network complexity in neonates with WMI may be indicative of delayed cortical maturation.

Findings from the current work suggest that WMI impacts WM microstructure in pathways underlying thalamocortical connectivity. Our findings indicate a more robust association between WMI and alterations in functional connectivity compared to microstructural connectivity. To determine whether these differences reflect the spectrum of WMI in this particular cohort of preterm neonates with infection, future work with larger cohorts of very preterm born neonates combining multimodal imaging methods are needed. Our findings may suggest that WMI may impact intrinsic activity in the thalamus resulting in alterations in thalamocortical connectivity more so than impacting white-matter microstructural pathways. The spatial extent of the injury was not a key predictor of alterations in functional and a structural connectivity. Quantitative mapping of WMI previously demonstrated that lesion location, not volume was a predictor of adverse outcome in preterms (Guo et al., 2017). In this work, WMI volume was largest in the right posterior thalamic radiations yet lesions in right superior and left posterior corona radiata and posterior thalamic radiations were more strongly associated with functional connectivity strength in early-acquired MRI scans. However, no differences in the lateralization of WMI volume was evident in the assessed WM fibre pathways. Thus, smaller lesions in WM pathways underlying parietal network connectivity may have had a compounding effect on early brain structure and function. Our findings raise the hypothesis that large lesions in one WM fibre pathway do not impact brain structure or function to the same degree as multiple lesions impacting parallel pathways. Future neuroimaging studies with larger cohorts and long-term follow up are needed to address the predictive ability of altered functional connectivity in preterm neonates.

Funding

Funding for this research was provided by operating grants from the Ontario Brain Institute, Ontario, Canada and the Canadian Institutes of Health Research (MOP-136966), Canada.

Acknowledgments

The authors wish to sincerely thank the families who participated in this research. Clinical data collection was provided by Angela Thompson, RN and Giselle Bordon, RN. The MRI research technologists Ruth Weiss and Tammy Rainer were essential for successful scanning of the neonates.

References

Back, S.A., Miller, S.P., 2014. Brain injury in premature neonates: a primary cerebral dysmaturation disorder? Ann. Neurol. 75 (4), 469–486.
Bassi, L., Chew, A., Merchant, N., Ball, G., Ramenghi, L., Boardman, J., Allsop, J.M., Doria, V., Arichi, T., Mosca, F., Edwards, A.D., Cowan, F.M., Rutherford, M.A., Counsell, S.J., 2011. Diffusion tensor imaging in preterm infants with punctate white matter lesions. Pediatr. Res. 69 (6), 561–566.
Beckmann, C.F., Smith, S.M., 2004. Probabilistic independent component analysis for functional magnetic resonance imaging. IEEE Trans. Med. Imaging 23 (2), 137–152.
Chau, V., Poskitt, K.J., McFadden, D.E., Bowen-Roberts, T., Synnes, A., Brant, R., Sargent, M.A., Soulikias, W., Miller, S.P., 2009. Effect of chorioamnionitis on brain development and injury in premature newborns. Ann. Neurol. 66 (2), 155–164.
Colonnese, M.T., Kaminska, A., Minlebaev, M., Milh, M., Bloem, B., Lescure, S., Moriette, G., Chiron, C., Ben-Ari, Y., Khazipov, R., 2010. A conserved switch in sensory processing prepares developing neocortex for vision. Neuron 67 (3), 480–498.
Conti, F., Fabri, M., Manzoni, T., 1986. Bilateral receptive fields and callosal connectivity of the body midline representation in the first somatosensory area of primates. Somatosens. Res. 3 (4), 273–289.
Cui, J., Tymofiyeva, O., Desikan, R., Flynn, T., Kim, H., Gano, D., Hess, C.P., Ferriero, D.M., Barkovich, A.J., Xu, D., 2017. Microstructure of the default mode network in preterm infants. AJNR Am. J. Neuroradiol. 38 (2), 343–348.
Dean, J.M., McClendon, E., Hansen, K., Azimi-Zonooz, A., Chen, K., Riddle, A., Gong, X., Sharifnia, E., Hagen, M., Ahmad, T., Leigland, L.A., Hohimer, A.R., Kroenke, C.D., Back, S.A., 2013. Prenatal cerebral ischemia disrupts MRI-defined cortical microstructure through disturbances in neuronal arborization. Sci. Transl. Med. 5 (168), 168ra167.
Doria, V., Beckmann, C.F., Arichi, T., Merchant, N., Groppo, M., Turkheimer, F.E., Counsell, S.J., Murgasova, M., Aljabar, P., Nunes, R.G., Larkman, D.J., Rees, G., Edwards, A.D., 2010. Emergence of resting state networks in the preterm human brain. Proc. Natl. Acad. Sci. U. S. A. 107 (46), 20015–20020.
Duerden, E.G., Foong, J., Chau, V., Branson, H., Poskitt, K.J., Grunau, R.E., Synnes, A., Zwicker, J.G., Miller, S.P., 2015. Tract-based spatial statistics in preterm-born neonates predicts cognitive and motor outcomes at 18 months. AJNR Am. J. Neuroradiol. 36 (8), 1565–1571.
Fransson, P., Skiold, B., Horsch, S., Nordell, A., Blennow, M., Lagercrantz, H., Aden, U., 2007. Resting-state networks in the infant brain. Proc. Natl. Acad. Sci. U. S. A. 104 (39), 15531–15536.
Guo, T., Winterburn, J.L., Pipitone, J., Duerden, E.G., Park, M.T., Chau, V., Poskitt, K.J., Grunau, R.E., Synnes, A., Miller, S.P., Mallar Chakravarty, M., 2015. Automatic segmentation of the hippocampus for preterm neonates from early-in-life to term-equivalent age. Neuroimage Clin. 9, 176–193.
Guo, T., Duerden, E.G., Adams, E., Chau, V., Branson, H.M., Chakravarty, M.M., Poskitt, K.J., Synnes, A., Grunau, R.E., Miller, S.P., 2017. Quantitative assessment of white matter injury in preterm neonates: association with outcomes. Neurology 88 (7), 614–622.
Haynes, R.L., Billiards, S.S., Borenstein, N.S., Volpe, J.J., Kinney, H.C., 2008. Diffuse axonal injury in periventricular leukomalacia as determined by apoptotic marker

fractin. Pediatr. Res. 63 (6), 656–661.
He, L., Parikh, N.A., 2015. Aberrant executive and frontoparietal functional connectivity in very preterm infants with diffuse white matter abnormalities. Pediatr. Neurol. 53 (4), 330–337.
He, L., Parikh, N.A., 2016. Brain functional network connectivity development in very preterm infants: the first six months. Early Hum. Dev. 98, 29–35.
Iwamura, Y., 2000. Bilateral receptive field neurons and callosal connections in the somatosensory cortex. Philos. Trans. R. Soc. Lond. Ser. B Biol. Sci. 355 (1394), 267–273.
Iwata, S., Nakamura, T., Hizume, E., Kihara, H., Takashima, S., Matsuishi, T., Iwata, O., 2012. Qualitative brain MRI at term and cognitive outcomes at 9 years after very preterm birth. Pediatrics 129 (5), e1138–e1147.
Jenkinson, M., Smith, S., 2001. A global optimisation method for robust affine registration of brain images. Med. Image Anal. 5 (2), 143–156.
Jenkinson, M., Bannister, P., Brady, M., Smith, S., 2002. Improved optimization for the robust and accurate linear registration and motion correction of brain images. NeuroImage 17 (2), 825–841.
Jenkinson, M., Beckmann, C.F., Behrens, T.E., Woolrich, M.W., Smith, S.M., 2012. Fsl. NeuroImage 62 (2), 782–790.
Kozberg, M.G., Ma, Y., Shaik, M.A., Kim, S.H., Hillman, E.M., 2016. Rapid postnatal expansion of neural networks occurs in an environment of altered neurovascular and neurometabolic coupling. J. Neurosci. 36 (25), 6704–6717.
Miller, S.P., Vigneron, D.B., Henry, R.G., Bohland, M.A., Ceppi-Cozzio, C., Hoffman, C., Newton, N., Partridge, J.C., Ferriero, D.M., Barkovich, A.J., 2002. Serial quantitative diffusion tensor MRI of the premature brain: development in newborns with and without injury. J. Magn. Reson. Imaging 16 (6), 621–632.
Miller, S.P., Ferriero, D.M., Leonard, C., Piecuch, R., Glidden, D.V., Partridge, J.C., Perez, M., Mukherjee, P., Vigneron, D.B., Barkovich, A.J., 2005. Early brain injury in premature newborns detected with magnetic resonance imaging is associated with adverse early neurodevelopmental outcome. J. Pediatr. 147 (5), 609–616.
Oishi, K., Mori, S., Donohue, P.K., Ernst, T., Anderson, L., Buchthal, S., Faria, A., Jiang, H., Li, X., Miller, M.I., van Zijl, P.C., Chang, L., 2011. Multi-contrast human neonatal brain atlas: application to normal neonate development analysis. NeuroImage 56 (1), 8–20.
van Pul, C., van Kooij, B.J., de Vries, L.S., Benders, M.J., Vilanova, A., Groenendaal, F., 2012. Quantitative fiber tracking in the corpus callosum and internal capsule reveals microstructural abnormalities in preterm infants at term-equivalent age. AJNR Am. J. Neuroradiol. 33 (4), 678–684.
Ramenghi, L.A., Fumagalli, M., Righini, A., Bassi, L., Groppo, M., Parazzini, C., Bianchini, E., Triulzi, F., Mosca, F., 2007. Magnetic resonance imaging assessment of brain maturation in preterm neonates with punctate white matter lesions. Neuroradiology 49 (2), 161–167.
Riddle, A., Maire, J., Gong, X., Chen, K.X., Kroenke, C.D., Hohimer, A.R., Back, S.A., 2012. Differential susceptibility to axonopathy in necrotic and non-necrotic perinatal white matter injury. Stroke 43 (1), 178–184.
Schneider, J., Duerden, E.G., Guo, T., Ng, K., Hagmann, P., Bickle Graz, M., Grunau, R.E., Chakravarty, M.M., Hüppi, P.S., Truttmann, A.C., Miller, S.P., 2018 Mar. Procedural pain and oral glucose in preterm neonates: brain development and sex-specific effects. Pain 159 (3), 515–525.
Smith, S.M., 2002. Fast robust automated brain extraction. Hum. Brain Mapp. 17 (3), 143–155.
Smith, S.M., Jenkinson, M., Johansen-Berg, H., Rueckert, D., Nichols, T.E., Mackay, C.E., Watkins, K.E., Ciccarelli, O., Cader, M.Z., Matthews, P.M., Behrens, T.E., 2006. Tract-based spatial statistics: voxelwise analysis of multi-subject diffusion data. NeuroImage 31 (4), 1487–1505.
Smyser, C.D., Inder, T.E., Shimony, J.S., Hill, J.E., Degnan, A.J., Snyder, A.Z., Neil, J.J., 2010. Longitudinal analysis of neural network development in preterm infants. Cereb. Cortex 20 (12), 2852–2862.
Smyser, C.D., Snyder, A.Z., Shimony, J.S., Blazey, T.M., Inder, T.E., Neil, J.J., 2013. Effects of white matter injury on resting state fMRI measures in prematurely born infants. PLoS One 8 (7), e68098.
Stoll, B.J., Hansen, N.I., Adams-Chapman, I., Fanaroff, A.A., Hintz, S.R., Vohr, B., Higgins, R.D., National Institute of Child H, Human Development Neonatal Research N, 2004. Neurodevelopmental and growth impairment among extremely low-birth-weight infants with neonatal infection. JAMA 292 (19), 2357–2365.
Toulmin, H., Beckmann, C.F., O'Muircheartaigh, J., Ball, G., Nongena, P., Makropoulos, A., Ederies, A., Counsell, S.J., Kennea, N., Arichi, T., Tusor, N., Rutherford, M.A., Azzopardi, D., Gonzalez-Cinca, N., Hajnal, J.V., Edwards, A.D., 2015. Specialization and integration of functional thalamocortical connectivity in the human infant. Proc. Natl. Acad. Sci. U. S. A. 112 (20), 6485–6490.
Woodward, L.J., Anderson, P.J., Austin, N.C., Howard, K., Inder, T.E., 2006. Neonatal MRI to predict neurodevelopmental outcomes in preterm infants. N. Engl. J. Med. 355 (7), 685–694.